Journal of Quantitative Spectroscopy & Radiative Transfer 146 (2014) 402–409

Contents lists available at ScienceDirect

Journal of Quantitative Spectroscopy & Radiative Transfer

journal homepage: www.elsevier.com/locate/jqsrt

Comparison of the pseudo-spectral time domain method and the discrete dipole approximation for light scattering by ice spheres

Derek I. Podowitz [a], Chao Liu [a,*], Ping Yang [a], Maxim A. Yurkin [b,c]

[a] Department of Atmospheric Sciences, Texas A&M University, College Station, TX 77843, USA
[b] Institute of Chemical Kinetics and Combustion SB RAS, Institutskaya 3, 630090 Novosibirsk, Russia
[c] Novosibirsk State University, Pirogova 2, 630090 Novosibirsk, Russia

ARTICLE INFO

Article history:
Received 5 November 2013
Received in revised form
13 February 2014
Accepted 18 February 2014
Available online 11 March 2014

Keywords:
Light scattering
PSTD
DDA

ABSTRACT

The pseudo-spectral time domain method (PSTD) and the discrete dipole approximation (DDA) are two popular numerically rigorous methods used to model the single-scattering properties of arbitrarily shaped dielectric particles. Stemming from a previous comparison made between the PSTD and DDA for non-absorptive particles, this study expands the comparison to include absorptive cases, and shows the relative strengths of the two methods for application to ice crystal light scattering. The scattering properties of spheres with realistic ice refractive indice, whose analytic solutions can be obtained by using the Lorenz–Mie theory, are considered. Refractive indices of ice at 30 wavelengths ranging from 0.2 μm to 100 μm are separated into three groups based on the imaginary parts of the refractive indices (i.e., $m_i < 10^{-3}$, $10^{-3} \le m_i \le 10^{-1}$, and $m_i > 10^{-1}$). The two methods are compared in terms of the computational time needed to reach the same accuracy. This study indicates that the performance of either the PSTD or DDA depends on both the real part and the imaginary part of the particle refractive index. For ice spheres with the imaginary part of the refractive index less than 10^{-3} and at size parameters exceeding 40, the PSTD is more efficient than the DDA. The PSTD also has a wider capability range for particles at larger sizes. At wavelengths where ice is moderately absorptive ($10^{-3} < m_i < 10^{-1}$ in this study), the critical size parameter decreases as the real part of the refractive index increases. At size parameters below the critical size parameter, the DDA outperforms the PSTD. Furthermore, when the ice becomes strongly absorptive, the DDA is approximately twice as fast as the PSTD for particles with size parameters reaching up to 100.

1. Introduction

Light scattering by dielectric particles is fundamental to the study of bio-optics, astrophysics, atmospheric radiative transfer simulations, and remote sensing applications [1]. Accurate and efficient computations of the single-scattering properties of various particles, e.g., red blood cells or atmospheric aerosol particles, are required in these fields of study. In single-scattering calculations, the 'size parameter', which is proportional to the particle size in comparison with the incident light wavelength, is crucially important and defined as $x = \pi L/\lambda$ (L is the maximum length of the particle, and λ is the incident wavelength). For particles much smaller than the incident wavelength, i.e., $x \ll 1$, the Rayleigh theory is generally

* Corresponding author.
E-mail address: chao_liu@tamu.edu (C. Liu).

http://dx.doi.org/10.1016/j.jqsrt.2014.02.032
0022-4073

applied, and in the large particle regime, $x \gg 1$, the geometric optics approximations are both useful and computationally feasible. In the intermediate region with x being in the few tens or hundreds, Maxwell's equations are normally solved numerically for light scattering by non-spherical particles, but the available analytic solution, i.e., the Lorenz–Mie theory [2,3], is only applicable for spheres and infinite cylinders.

Various numerical algorithms have been developed and applied to model the single-scattering properties of dielectric particles in the resonant region, i.e., the T-matrix [4–7], the discrete dipole approximation (DDA) [8–10], the finite-difference time domain method (FDTD) [11–13], and the pseudo-spectral time domain method (PSTD) [14–16]. This study focuses on two popular approaches: the PSTD and the DDA. The PSTD, which solves Maxwell's curl equations in the time domain, uses a spectral method to calculate spatial derivatives; whereas, the DDA solves an electromagnetic integral equation in the frequency domain. Note that the DDA has been extended to consider magnetic dipoles for applications to material science [17]. The two methods discretize the particles using either grid cells or dipoles in the spatial domain, and can be applied to particles with arbitrary shapes and compositions. Both the PSTD and DDA have been widely applied to simulate the scattering properties of atmospheric particles, e.g., ice crystals [15,18,19] and dust particles [20–23], and have been compared with other methods such as the FDTD [23,24] and T-matrix [16,25]. The implementations of the two methods have been parallelized and applied to particles much larger than the incident wavelength. Liu et al. [16] used the PSTD to simulate the light scattering by spheres with refractive indices of ice and size parameters up to 200 and by randomly oriented non-spherical particles with size parameters over 100. The efficiency of the DDA depends strongly on the particle refractive index, and maximum size parameters of 130 and 320 for spheres with respective refractive indices of 1.2 and 1.05 have been achieved [26,27].

Although sharing a similar range of applicability for light scattering simulations, the efficiency and accuracy of the PSTD and DDA show substantial variations at different refractive indices and particle sizes. Liu et al. [28] have studied the capabilities and relative strengths of the PSTD and DDA for light scattering by spheres and spheroids. With the exact scattering properties of spheres given by the Lorenz–Mie theory, the same accuracy criteria were prescribed for the two methods, and the computational time was compared in a fair manner. For a small refractive index, a critical size parameter was found below which the DDA outperformed the PSTD. The value of the critical size parameter decreased from 80 to 30 as the refractive index increased from 1.2 to 1.4. For particles with refractive indices larger than 1.4, the PSTD became more efficient than the DDA for spheres with size parameters larger than 10 and had a broader range of applicability for large sized particles. However, Liu et al. [28] focused on the real part of refractive index (with the imaginary part of the refractive index assumed to be 0). Meanwhile, the PSTD showed much higher accuracy for absorptive particles than those of non-absorptive cases [16], and Yurkin et al. [24] found that the performance of the DDA was also significantly affected by the imaginary part of the refractive index. As realistic particles are always absorptive to some degree, a comparison between the PSTD and DDA for absorbing refractive indices, which was mentioned as future work by both Yurkin et al. [24] and Liu et al. [28], is more meaningful from a practical application perspective.

This study presents an expanded comparison between the PSTD and DDA by using realistic refractive indices of ice at wavelengths ranging from 0.2 μm to 100 μm. The present results are intended to show the relative performances of the two methods for both non-absorptive and absorptive cases, and, thus, to provide a reference for further applications of ice crystal single-scattering simulations. Section 2 details the methods for the comparison, and Section 3 discusses the results. Section 4 summarizes the study.

2. Comparison between the PSTD and DDA

Both the PSTD and DDA show a wide range of applications to light scattering by ice crystals within cirrus clouds. The accuracy and efficiency of the PSTD and DDA simulations become extremely important, because various particle geometries, sizes, and refractive indices (at different wavelengths) need to be considered for atmospheric applications. The appropriate model will not only save significant computational resources, but will also provide more robust and accurate results. This study is intended to provide a detailed comparison of the two methods for light scattering simulations over a wide range of particle sizes and refractive indices. The ADDA code (v.1.1), developed by Yurkin and Hoekstra [27], and the PSTD code, improved and parallelized by Liu et al. [16,28], are used for the comparison. A more detailed discussion of the two implementations can be found in Liu et al. [28], and the basic simulation variables and parameters are kept the same as in their study. In particular, the ADDA was run with default settings, including the lattice dispersion relation (LDR) formulation and the quasi-minimal residual (QMR) iterative solver. The only difference is the threshold of the latter, which was set to 10^{-3}. We note that the ADDA code has several options to choose the DDA formulations and the iterative solver, the optimizing of which may have a profound influence on the code performance [28,29]; however, such optimization is out of scope of this paper.

By discretizing the scattering particles using grid cells (PSTD) or dipoles (DDA), the PSTD and DDA have almost no limitations on the particle geometries. However, to quantify the accuracies of the PSTD and DDA for a fair comparison, the single-scattering properties of spheres are simulated, because exact solutions can be given by the Lorenz–Mie theory. The same accuracy criteria for the extinction efficiency (Q_{ext}) and the phase function (P_{11}) are prescribed, and computational times used by the two methods with the same resources are directly compared. The computational times depend on the size of the computational domain, i.e., the number of grid cells or dipoles, and the number of time steps in the time domain simulations for the PSTD or iterations by the iterative solver for the DDA (N_{iter}). The number of time steps in the PSTD simulations will be specified as N_{trip} in this study,

and $N_{trip}=1$ refers to the time steps used for the electromagnetic fields to travel through the particle (i.e., the maximum distance of the particle in the incident direction). For a given particle size, the computational domain is determined by the spatial resolution, i.e., the number of grid cells or dipoles per wavelength ($\lambda/\Delta x$ for the PSTD and dipole per lambda, i.e. dpl, for the DDA, where Δx is the size of the grid cell/dipole). The accuracy of each method increases as the spatial resolution increases, and we increase the spatial resolution until either the prescribed accuracy criteria are achieved or the simulation becomes too time-consuming. We require the relative errors (RE) of Q_{ext} to be less than 2% and the root mean square relative errors (RMSRE) of $P_{11}(\theta)$ to be less than 30%, where θ is the scattering angle ranging from 0° to 180°. Considering the large number of simulations and the computational time, the accuracy criteria in this study are larger than those in previous studies [24,28], but both methods can achieve much higher accuracy with larger spatial resolution and longer computational time. All simulations are carried out using a single node containing 8 64-bit 2.8 GHz processors on the EOS cluster at the Texas A&M Supercomputing Facility. In addition to the accuracy criteria, all simulations are limited to within 48 h (wall time), i.e., if the prescribed accuracy criteria are not achieved within 48 h, the spatial resolutions will not be further increased.

This study uses the realistic ice refractive indices for spheres, and can serve as a guide for many further applications. We select 30 refractive indices at wavelengths ranging from 0.2 to 100.0 μm, and, to demonstrate the effects of the imaginary part of refractive index more clearly, the 30 refractive indices are chosen and separated into three groups based on the values of their imaginary parts, i.e., degree of absorption: weakly absorptive cases (Group 1: $m_i < 10^{-3}$); moderately absorptive cases (Group 2: $10^{-3} \le m_i \le 10^{-1}$); and, strongly absorptive cases (Group 3: $m_i > 10^{-1}$). Each of the three groups has 10 different refractive indices, of which most are chosen at the maxima or minima of either the real or imaginary part of the ice refractive index. Note that the absorption of the particle depends on both its refractive index and size, and the grouping here is not generally related to the degree of particle absorption but for the convenience of the study discussion. For each of the 30 wavelengths, eight size parameters from 5 to 100 (defined as $x=2\pi r/\lambda$ for a sphere, where r is the radius) are considered, i.e., 5, 10, 20, 30, 40, 60, 80, and 100. The refractive indices of ice given by Warren and Brandt [30] are used, and Fig. 1(a) and (b) shows the real part m_r and imaginary part m_i of the ice refractive indices. The colored circles in the figure specify the selected refractive indices/wavelengths in the three defined absorptive regions; red corresponds to the weakly absorptive case, blue to the moderately absorptive case, and green to the strongly absorptive case. The imaginary part of the refractive index as a function of the corresponding real part is shown in Fig. 1(c).

3. Results

This study compares the two methods at 30 different refractive indices and eight different sizes, and a total of 480 results will be obtained for any scattering property. To show all the data in the paper would be extremely tedious, and the data for a single refractive index and a single size is meaningless for general application of the two methods. Thus, as previously mentioned, we separated the 30 refractive indices into three groups based on their imaginary parts, and found that the variations in the performance of the two methods

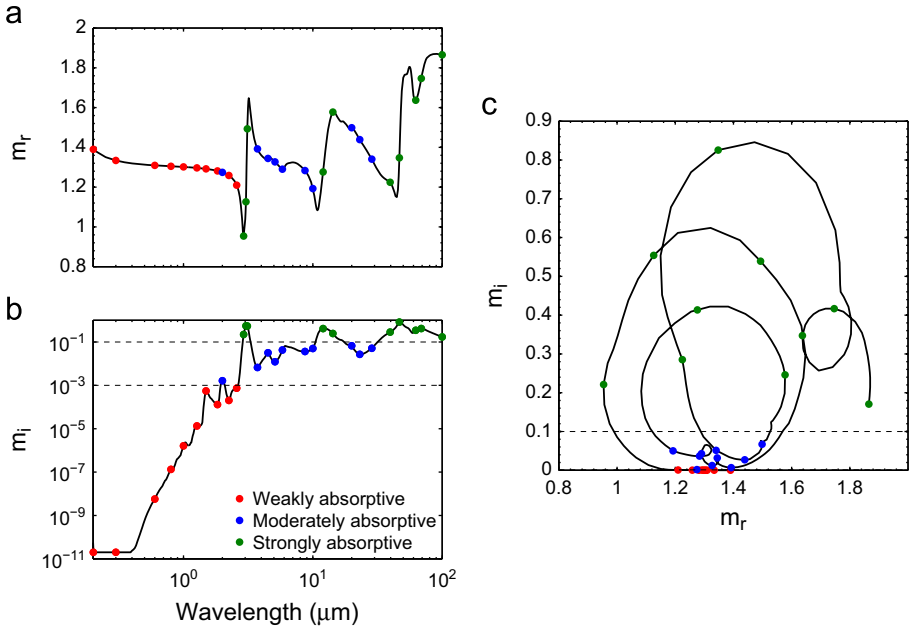

Fig. 1. (a) and (b) illustrates the real and imaginary parts of the ice refractive indices, and the three groups used for the comparison. (c) Correlation of the real and imaginary part of the ice refractive index. (For interpretation of the references to color in this figure, the reader is referred to the web version of this article.)

within each group is relatively minor compared with the variations among different sizes or groups. Consequently, we focus on the relative performance of the two methods in each group, and discuss the results based on the three groups by illustrating either the values averaged over each group or a single example representing the group. The results provide a more general and precise idea of the effect of the imaginary parts of the refractive indices on light scattering simulations, and may be used for further applications of the two methods.

To be more specific, we consider only the cases in which the two accuracy criteria were both achieved within 48 h by either method, and define the weighting function η_i in the form of

$$\eta_i = \begin{cases} 1, & \text{the method meets both accuracy criteria,} \\ 0, & \text{the method does not meet at least one of accuracy criteria.} \end{cases} \tag{1}$$

Thus, for each group, to illustrate the performance of the method, the averaged parameter at a particular group and size is given by

$$\overline{Q} = \frac{\sum_{i=1}^{10} Q_i \eta_i}{\sum_{i=1}^{10} \eta_i}, \tag{2}$$

where Q_i is the value given by the PSTD or DDA for the modeled spheres with the ith refractive indices in the group, and $\overline{Q}$ is the averaged value. The quantities in which we are interested include the RE of extinction efficiency, the RMSRE of phase function, the computational time t, the spatial resolution, the N_{trip} for the PSTD, and the N_{iter} for the DDA. In Eq. (2), the normalization parameter (the denominator) is represented as $\Sigma = \sum_{i=1}^{10} \eta_i$, and is the number of cases in which the method achieves the two prescribed accuracy criteria in the particular group and size. The value of Σ is an important value to demonstrate the capability of the methods (Fig. 2 panel (c)).

Fig. 2 illustrates several key parameters for the comparisons between the PSTD and DDA of the three groups as functions of the size parameter, and includes the two accuracy parameters (panel (a) for the RE of extinction efficiency and panel (b) for the RMSRE of phase function), Σ (panel (c), i.e., the number of cases in which the PSTD or DDA achieved the two prescribed criteria), and the ratio of computational times of the PSTD to DDA at each size parameter (panel (d)). The values shown in Fig. 2 are averaged or summed over each absorptive group, and indicate the overall accuracy and performance of the two methods. The solid lines are the PSTD results, and the dashed lines are the DDA results. Fig. 2 clearly illustrates that both the PSTD and DDA show higher accuracy as the imaginary part of the refractive index increases, and the averaged RE of Q_{ext} and RMSRE of P_{11} are under 0.6% and 15%, respectively, except for spheres in Group 1 with weak absorption but large size parameters. The RE of Q_{ext} shows

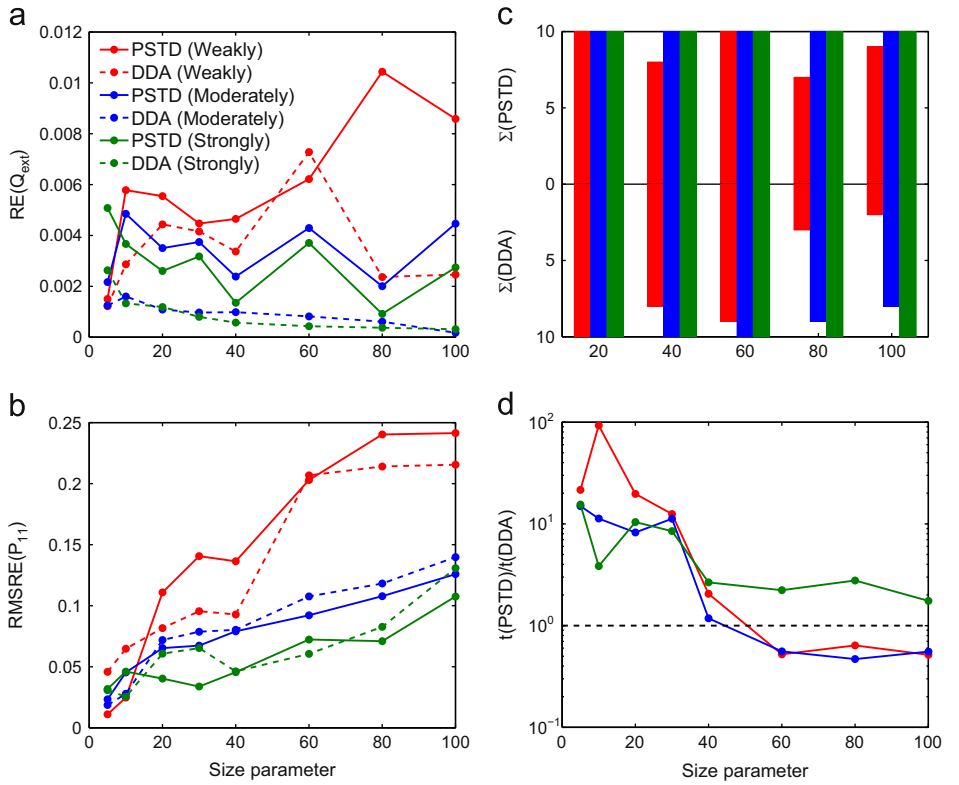

Fig. 2. (a) and (b) illustrates the averaged relative errors of the extinction efficiency and the RMS relative errors of the P_{11} phase function for spheres with the refractive indices grouped by their imaginary part. (c) The number of cases the PSTD or DDA meets both accuracy criteria. (d) The ratios of computational times of the PSTD to DDA as a function of particle size parameters for the different absorptive conditions. (For interpretation of the references to color in this figure, the reader is referred to the web version of this article.)

no dependence on particle size, whereas the RMSRE of P_{11} roughly increases as the size parameter increases. The DDA gives smaller REs for the Q_{ext}, but similar errors are obtained by the two methods for the RMSRE of P_{11}. Note, that in order to be able to generalize, these accuracy trends should be considered together with the particular levels of discretization, see Fig. 3(a) and (c). The normalization parameter Σ is shown in Fig. 2(c) (only for size parameters 20, 40, 60, 80, and 100). The upper part in Fig. 2(c) shows the PSTD results, and the lower part shows the DDA results. The PSTD achieves all 10 cases with moderately and strongly absorptive spheres (blue and green bars, respectively), but the DDA fails in three cases with moderate absorption and size parameters of 80 and 100. However, the DDA is significantly limited for spheres with size parameters of 80 and 100 and small imaginary parts of the refractive indices (smaller than 10^{-3}) with only 3 and 2 cases respectively achieving both criteria, but the PSTD performs constantly and accurately for those spheres and fails to achieve the criteria in only three cases at a size parameter of 80 and one case at a size parameter of 100. A similar conclusion was reached for the non-absorptive cases by Liu et al. [28]. With the same accuracy prescribed criteria, the computational time of the two methods can be directly compared to show their relative strengths. Panel (d) of Fig. 2 shows the ratios of the PSTD computational time to that of the DDA. The same averaging calculations as Eq. (2) are carried out for the computational time of each method, and the figure shows the ratios of the averaged time. When the size parameter of the spheres is less than 40, the DDA is approximately one order of magnitude faster than the PSTD; however, the two methods show quite different performances for the three absorptive groups as the size parameter increases. The PSTD becomes the more efficient method for the weakly and moderately absorptive spheres at large size ranges, while the DDA is approximately two times faster than the PSTD for the strongly-absorptive spheres with large size parameters. Considering the results shown in Fig. 2 and the conclusions from Liu et al. [28], the imaginary part of refractive index does play an important role on both the accuracy and efficiency of single-scattering simulations.

To gain a better understanding on the methods' performance and show the effects of the particle absorption on the two numerical models, we provide internal computational parameters of the PSTD and DDA in Fig. 3. Panels (a) and (c) describe the dependence of spatial resolution on x, averaged over three groups of refractive indices. Variation within each group (data not shown) does not affect the general trend. One can see that, for the PSTD, the spatial resolution $\lambda/\Delta x$ generally decreases as the size parameter increases, from approximately 30 for the small-sized particles to 10 for spheres with a size parameter of 100. The discretization level of the DDA shows a similar trend, but with a certain dependence on m_i for small x. The lower panels of Fig. 3 show (b) N_{trip} for the PSTD simulations and (d) N_{iter} in the DDA versus x, also with values averaged over each absorptive group. For the

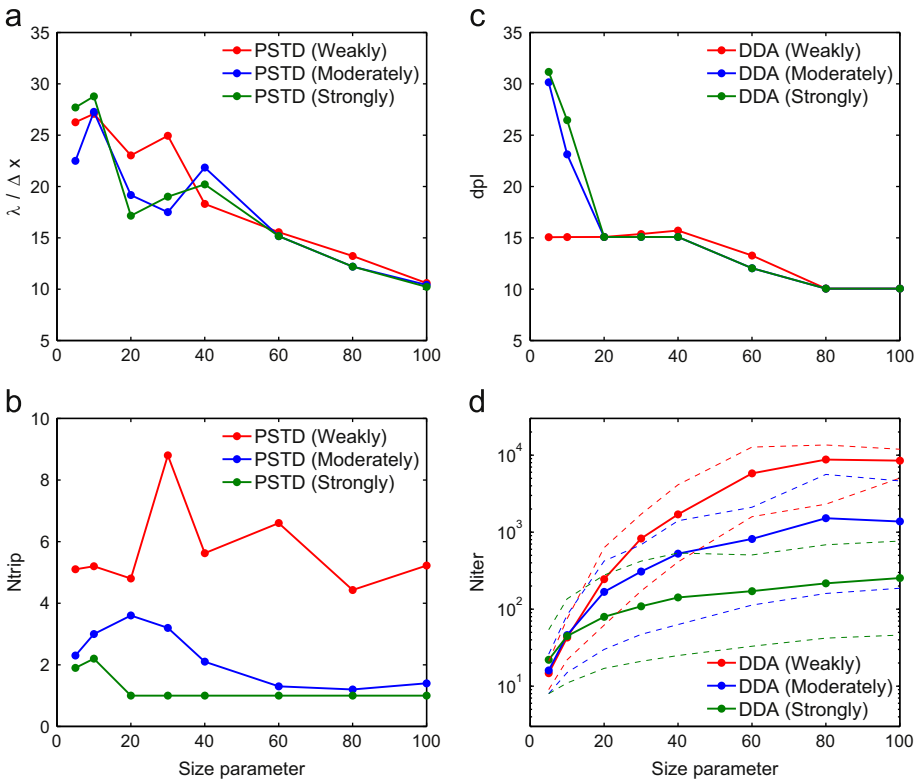

Fig. 3. (a) and (c) Averaged spatial resolution for the PSTD and DDA, given as number of volume elements per the wavelength ($\lambda/\Delta x$ and dpl) versus x, with the refractive indices grouped by their imaginary part. (b) The number of N_{trip} for the PSTD, and (d) the number of iterations for the DDA, showing mean (solid line) and extremum (dashed lines) values for each group of refractive indices.

weakly absorptive spheres, it takes the incident pulse approximately $N_{trip}=5$ to attenuate in the PSTD simulations. However, much less time is used for the moderately and strongly absorptive groups, because the energy is rapidly absorbed by the particle. The required N_{trip} for the PSTD simulations at each absorptive group does not show a trend as to particle size parameter. By contrast, for the DDA, the variation inside each group of refractive indices is significant, since N_{iter} largely depends on m_r [24,26,28]. Therefore, we plotted the averaged values as well as the minimum and maximum N_{iter} inside each group. Note that flattening of the red curves (weak absorption) for large x is an artifact caused by the limitation of the computational time (largest values of N_{iter} correspond to discarded non-converged cases). The most important feature in Fig. 3(d) is that the slope of the curves significantly decreases with increasing m_i, and the effect on the simulation time is much more significant than that of N_{trip} in the PSTD simulations. In particular, N_{iter} for the strong absorptive group scales almost linearly with x, which is very favorable for the DDA and is the same as the scaling of total time steps in the PSTD, and allows the DDA to outperform the PSTD for this case. Moreover, the relation is expected to hold for larger sizes as well, as long as linear scaling of N_{iter} holds for the DDA. Mathematical insight into the effect of absorption on N_{iter} can be gained from consideration of the spectrum of the volume-integral scattering operator [31]; however, a simple phenomenological explanation is available. Absorption dampens interaction of distant dipoles, and effectively reduces the size of the particle with respect to the strength of overall dipole interaction, which in turn determines the condition number of the interaction matrix.

A further comparison of the numerical performance of the two methods is illustrated in Fig. 4. The figure shows examples of the phase function P_{11} given by the PSTD and DDA from each absorptive group at a size parameter of 100 (from upper to lower panels, the refractive indices are $1.31+5.73\times10^{-9}$i, $1.39+6.67\times10^{-3}$i, and $1.28+4.13\times10^{-1}$i at wavelengths 0.60, 3.73 and 12.0 μm), and, for comparison, the exact solutions from the Lorenz–Mie theory are illustrated. The RMSREs of the phase function given by the PSTD and DDA are listed in the figure, and the relative errors as a function of the scattering angle are shown in the right panels. The DDA does not achieve the accuracy criterion of the RMSRE with values of 40.5% and 36.4% for the weakly and moderately absorptive cases. At a large size parameter of $x=100$, both the PSTD and DDA show relative errors less than

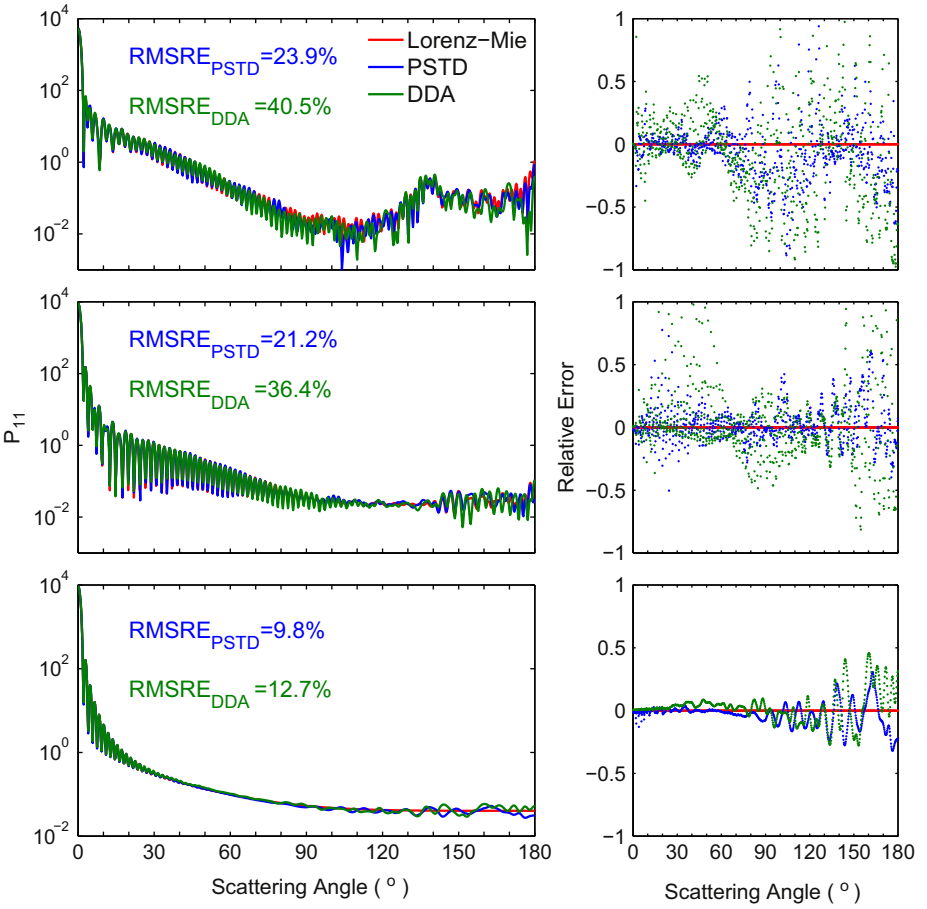

Fig. 4. The phase functions (left panels) and their relative errors (right panels) for spheres with $x=100$ at three wavelengths with weak (upper panels, 0.60 μm, $m=1.31+5.73\times10^{-9}$i), moderate (middle panels, 3.73 μm, $m=1.39+6.67\times10^{-3}$i), and strong absorption (lower panels, 12.0 μm, $m=1.28+4.13\times10^{-1}$i).

50% at most scattering angles when the absorption is not strong, but the relative errors become as large as 100% near the scattering angles where sharp troughs or peaks occur in the phase function. When the sphere becomes strongly absorptive, both methods show improved accuracy for the backward scattering except for slight oscillations that are not shown in the Lorenz–Mie results.

To be more specific, this study compares the PSTD and DDA to determine which method is the preferable one when considering both the accuracy and computational time at each wavelength and size parameter. Fig. 5 illustrates the relative performance of the two methods on light scattering by ice particles at the 30 wavelengths and eight sizes (the only figure illustrating the variations among each absorptive group). The three background colors correspond to the three groups of imaginary parts of the ice refractive indices, and the color becomes darker as the absorption becomes stronger. The circles in the figure illustrate the spheres chosen for comparison at the corresponding wavelength (x-axis) and size parameter (y-axis). The color of the circle is determined by the accuracy performance of the two methods. The green circles covering over 90% of the comparisons (220 out of 240) correspond to cases at which both numerical methods met the two accuracy criteria ($\mathrm{RE}(Q_{\mathrm{ext}}) \le 2\%$ and $\mathrm{RMSRE}(P_{11}) \le 30\%$); whereas, the 6 red cases are those in which neither method could reach the set criteria. The 14 spheres represented by the blue circles are those in which the PSTD achieved both accuracy criteria, but the DDA did not (given the 48 h time limit). The 14 cases are mainly in the large size regime and at visible/near infrared wavelengths. Overall, the two methods show robust performances for small particles with size parameters less than 40 and for the strongly absorptive particles of all sizes. When both the PSTD and DDA achieve the same criteria, the relative performances are determined by the computational time, and are illustrated by the filling of the circles. The solid circles indicate the cases in which the PSTD is faster than the DDA; the hollow circles are for those cases in which the DDA is more efficient. The DDA shows great performance for the small-sized spheres with size parameters equal or less than 30 and is the faster method when the same accuracy is achieved by the PSTD. However, the results become more complicated as the particle gets larger. The PSTD is faster than the DDA at computing the single-scattering properties of spheres with size parameters greater than approximately 50 at wavelengths with the imaginary part of the ice refractive index less than 10^{-3} (region with lightest background). There is a critical size parameter, above which the PSTD remains more efficient for the moderately absorptive cases ($10^{-3} \le m_{\mathrm{i}} \le 10^{-1}$). The critical size parameter ranges from 30 to 80, depends on the real part of the refractive index, and decreases as m_{r} increases. However, as the ice becomes strongly absorptive with m_{i} larger than 10^{-1} (region with darkest background), the DDA shows much higher accuracy and efficiency compared with the PSTD, except at wavelength 100 μm with the real part of the refractive index as large as 1.8.

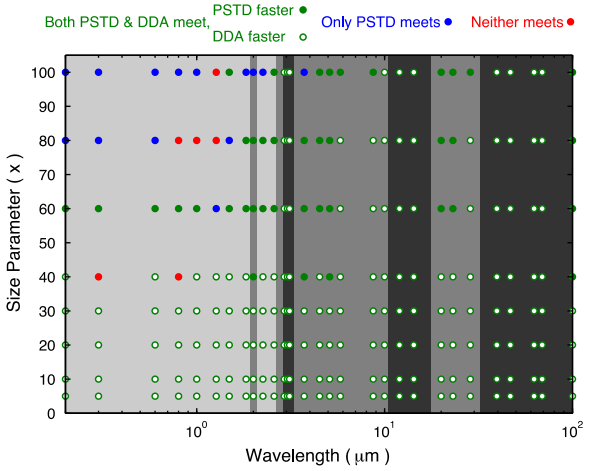

Fig. 5. The relative performance of the PSTD and DDA for ice spheres with different size parameters and wavelengths from 0.2 to 100 μm. The background indicates the imaginary parts of ice refractive indices at their corresponding wavelengths (light region: $m_{\mathrm{i}} < 10^{-3}$; dark region: $m_{\mathrm{i}} > 10^{-1}$; and, remainder: m_{i} between 10^{-3} and 10^{-1}). Solid circles indicate that the PSTD is faster for the spheres at the corresponding size parameter and wavelengths; whereas, the hollow circles are for those in which the DDA is faster. The different colors illustrate whether the PSTD or DDA results meet the accuracy criteria.

4. Conclusion

This study expands the comparison between the PSTD and DDA for light scattering by absorptive particles with realistic ice refractive indices. By employing the same accuracy criteria for light scattering properties of spheres, the computational times used by the PSTD and DDA indicate their relative performances. Both methods show excellent efficiency and accuracy over a wide range of particle sizes and refractive indices, and are applicable to ice particles with size parameters up to 100, except for the DDA at visible and near infrared regions. Furthermore, the efficiency of the two methods is found to depend on both the real and imaginary parts of the refractive index. For weakly absorptive cases, i.e. $m_{\mathrm{i}} < 10^{-3}$ (ice at visible and near infrared wavelengths), the PSTD is faster than the DDA for spheres with size parameters larger than approximately 50, and the DDA encounters difficulties with both efficiency and accuracy for larger particles. These conclusions are coincident with those from Liu et al. [28], which considered only the real part of the refractive index. However, as the particles become more absorptive with the imaginary part of the refractive index between 10^{-3} and 10^{-1} and the corresponding real part varying from 1.2 to 1.5, the PSTD can be the more efficient method for spheres larger than a critical size parameter. The value of the critical size parameter increases as m_{r} decreases. For the strongly absorptive cases, the DDA is the more efficient method for all spheres with size parameters ranging from 5 to 100, except for spheres with the real part of the refractive index being almost 1.8 at the 100 μm wavelength.

This study shows the relative performance of the two widely used numerical methods, i.e., the PSTD and DDA, and can serve as a reference for the application of the two methods on light scattering simulations. The appropriate

method can provide more accurate results with less computational resources. Furthermore, the conclusions obtained are not limited to ice crystals and can be generally applied for all particles with a similar range of refractive indices.

Acknowledgments

The research was partially supported by NSF (ATM-0803779 and AGS-1338440) and the endowment funds related to the David Bullock Harris Chair in Geosciences at the College of Geosciences, Texas A&M University. All computations were carried out at the Texas A&M University Supercomputing Facility, and we gratefully acknowledge the assistance of Facility staff in porting our codes. M.A. Yu acknowledges support by the Russian Foundation for Basic Research (grant 12-04-00737-a), Ministry of Education and Science of the Russian Federation and Stipend of the President of Russian Federation for Young Scientists.

References

[1] Mishchenko MI, Hovenier JW, Travis LD. Light scattering by nonspherical particle: theory, measurements, and geophysical applications. San Diego: Academic Press; 2000.
[2] Mie G. Beitrage zur optic truber medien, speziell kolloidaler metallosungen. Ann Phys 1908;25:337–445.
[3] Bohren CF, Huffman DR. Absorption and scattering of light by small particles. New York: Wiley; 1983.
[4] Waterman PC. Matrix formulation of electromagnetic scattering. Proc IEEE 1965;53:805–12.
[5] Waterman PC. Symmetry, unitarity, and geometry in electromagnetic scattering. Phys Rev D 1971;3:825–39.
[6] Mishchenko MI, Travis LD, Mackowski DW. T-matrix computations of light scattering by nonspherical particles: a review. J Quant Spectrosc Radiat Transf 1996;55:535–75.
[7] Mishchenko MI, Travis LD. Capabilities and limitations of a current FORTRAN implementation of the T-matrix method for randomly oriented, rotationally symmetric scatterer. J Quant Spectrosc Radiat Transf 1998;60:309–24.
[8] Purcell EM, Pennypacker CR. Scattering and absorption of light by nonspherical dielectric grains. Astrophys J 1973;186:705–14.
[9] Draine BT, Flatau PJ. Discrete-dipole approximation for scattering calculations. J Opt Soc Am A 1994;11:1491–9.
[10] Yurkin MA, Hoekstra AG. The discrete dipole approximation: an overview and recent developments. J Quant Spectrosc Radiat Transf 2007;106:558–89.
[11] Yee SK. Numerical solution of initial boundary value problems involving Maxwell's equations in isotropic media. IEEE Trans Antennas Propag 1966;14:302–7.
[12] Yang P, Liou KN. Finite-difference time domain method for light scattering by small ice crystals in three-dimensional space. J Opt Soc Am A 1996;13:2072–85.
[13] Sun W, Fu Q, Chen Z. Finite-difference time-domain solution of light scattering by dielectric particles with a perfectly matched layer absorbing boundary condition. Appl Opt 1999;38:3141–51.
[14] Liu QH. The PSTD algorithm: a time-domain method requiring only two cells per wavelength. Microw Opt Technol Lett 1997;15:158–65.
[15] Chen G, Yang P, Kattawar GW. Application of the pseudospectral time-domain method to the scattering of light by nonspherical particles. J Opt Soc Am A 2008;25:785–90.
[16] Liu C, Panetta RL, Yang P. Application of the pseudo-spectral time domain method to compute particle single-scattering properties for size parameters up to 200. J Quant Spectrosc Radiat Transf 2012;113:1728–40.
[17] You Y, Kattawar GW, Zhai PW, Yang P. Invisibility cloaks for irregular particles using coordinate transformations. Opt Express 2008;16:6134–45.
[18] Yang P, Bi L, Baum BA, Liou KN, Kattawar GW, Mishchenko MI, et al. Spectrally consistent scattering, absorption, and polarization properties of atmospheric ice crystals at wavelengths from 0.2 to 100 μm. J Atmos Sci 2013;70:330–47.
[19] Liu C, Panetta RL, Yang P. The effects of surface roughness on the scattering properties of hexagonal columns with sizes from the Rayleigh to the geometric optics regimes. J Quant Spectrosc Radiat Transfer 2013;129:169–85.
[20] Bi L, Yang P, Kattawar GW, Kahn R. Modeling optical properties of mineral aerosol particles by using nonsymmetric hexahedra. Appl Opt 2010;49:334–42.
[21] Zubko E, Muinonen K, Munoz O, Nousiainen T, Shkuratov Y, Sun W, et al. Light scattering by feldspar particles: comparison of model agglomerate debris particles with laboratory samples. J Quant Spectrosc Radiat Transf 2013;131:175–87.
[22] Liu C, Panetta RL, Yang P, Macke A, Baran AJ. Modeling the scattering properties of mineral aerosols using concave fractal polyhedral. Appl Opt 2013;52:640–52.
[23] Sun W, Vidden G, Fu Q, Hu Y. Scattered-field FDTD and PSTD algorithms with CPML absorbing boundary conditions for light scattering by aerosols. J Quant Spectrosc Radiat Transf 2013;131:166–74.
[24] Yurkin MA, Hoekstra AG, Brock RS, Lu JQ. Systematic comparison of the discrete dipole approximation and the finite difference time domain method for large dielectric scatterers. Opt Express 2007;15:17902–11.
[25] Yurkin MA, Kahnert M. Light scattering by a cube: accuracy limits of the discrete dipole approximation and the T-matrix method. J Quant Spectrosc Radiat Transf 2013;123:176–83.
[26] Yurkin MA, Maltsev VP, Hoekstra AG. The discrete dipole approximation for simulation of light scattering by particles much larger than the wavelength. J Quant Spectrosc Radiat Transf 2007;106:546–57.
[27] Yurkin MA, Hoekstra AG. The discrete-dipole-approximation code ADDA: capabilities and known limitations. J Quant Spectrosc Radiat Transf 2011;112:2234–47.
[28] Liu C, Bi L, Panetta RL, Yang P, Yurkin MA. Comparison between the pseudo-spectral time domain method and the discrete dipole approximation for light scattering simulations. Opt Express 2012;20:16763–76.
[29] Yurkin MA, Min M, Hoekstra AG. Application of the discrete dipole approximation to very large refractive indices: filtered coupled dipoles revived. Phys Rev E 2010;82:036703.
[30] Warren SG, Brandt RE. Optical constants of ice from the ultraviolet to the microwave: a revised compilation. J Geophys Res 2008;113:D14220. http://dx.doi.org/10.1029/2007JD009744.
[31] Budko NV, Samokhin AB. Spectrum of the volume integral operator of electromagnetic scattering. SIAM J Sci Comput 2006;28:682–700.